Hindawi
Mobile Information Systems
Volume 2022, Article ID 1794852, 11 pages
https://doi.org/10.1155/2022/1794852

Research Article

Manipulator Mechanical System Design and Operation Algorithm Based on Multisensor Fusion

Jian Jiao[1] **and Chengdong Li**[2]

[1]*Automobile Engineering Department, Lanzhou Institute of Technology, Lanzhou, Gansu 730050, China*
[2]*Gansu Xinghe Communication Technology, Lanzhou, Gansu 730050, China*

Correspondence should be addressed to Jian Jiao; jiaoj@lzit.edu.cn

Received 27 January 2022; Revised 22 March 2022; Accepted 28 March 2022; Published 27 April 2022

Academic Editor: Hye-jin Kim

With the advancement of modern technology and the improvement of the level of social productivity, people are paying more and more attention to the reduction of labor intensity and the change of working environment. At the same time, in order to explore the application of multisensor fusion in the design and operation algorithm of manipulator mechanical system, we first introduced the big data fusion, proposed the multisensor data fusion algorithm, and analyzed the gradient descent method, auxiliary filtering method, and Kalman filter. Finally, the rated motion parameters of each axis motor of the manipulator are analyzed, and at the same time, the motion state of each axis motor of the manipulator under nonrated speed is analyzed. The research proposal in this paper is aimed at contributing to improving productivity.

1. Introduction

With the increasing development of science and technology in contemporary society, automated robotic technology has begun to be applied to all aspects of human production and life. As a part of industrial robots, manipulators can play more important roles in manufacturing and other fields, not only can greatly improve production efficiency but also can liberate people from tedious work. For example, in the intelligent warehouse management system, robot hands can be used to complete palletizing. The main purpose of palletizing is to make the warehousing, outgoing, and transfer activities of goods to be completed with pallets as a unit, which greatly improves the efficiency of the logistics delivery of goods.

With the development of modern technology and the improvement of social productivity, people are paying more attention to the reduction of labor intensity and the change of working environment. Commercial packaging on industrial assembly lines such as food, medicine, and home appliances has increasingly higher requirements for product quality and work efficiency. However, traditional manual packaging technology can no longer meet the needs of modern manufacturing due to low work efficiency and packaging product quality. Since the current domestic and foreign automatic boxing manipulators are mainly imported, the domestic automatic boxing manipulator production enterprises are relatively small, and the demand for automatic boxing manipulators in the domestic and foreign markets is also considerable. Therefore, the contradiction between the low-efficiency manual boxing hand and the increasing number of commercial production enterprises has become increasingly intensified, making the research and development of the automatic boxing manipulator produce huge social and economic benefits and practical significance. Based on the multisensor fusion, this paper conducts research and discussion on the design and operation algorithm of the manipulator mechanical system, in order to make a certain contribution in improving the level of productivity.

The innovations of this paper are embodied in the following: (1) the concept of big data fusion is proposed; (2) the multisensor data fusion algorithm is proposed. The data fusion algorithm can remove redundant information while retaining complementary information to achieve the best

estimation of information. (3) The rated motion parameters of each axis motor of the manipulator are analyzed. (4) The motion status of each axis motor of the manipulator under nonrated speed is also analyzed and studied.

2. Related Work

According to the research progress at home and abroad, different scholars also have a certain degree of cooperation in multisensor fusion and manipulator mechanical system design. Yi et al. proposed a new method of multistatic radar system distributed multitarget tracking. This method is based on the intersection of generalized covariances of multiobjective densities and is used for the fusion of posterior information in multiobjective Bayesian filtering schemes [1]. Lu and Zhou research proposed a new data fusion algorithm in sensor networks, which has both set membership and random Gaussian measurement uncertainty. The suggested approach is based on the combination of ellipsoidal algorithm theory and data reduction method [2]. Benli et al. proposed thermal multisensor fusion (TMF) for collaborative robots to overcome the limitations of independent robots. It proves that TMF enhances the precise target positioning ability of collaborative robots by providing a wide range of FOV and provides precise target positioning for collaborative robots [3]. Shi et al. presented the elaborate robotic design of the vacuum-compatible arm and actuator and investigated the flexibility of the manipulator by experimental and model recognition algorithms to estimate the distortion [4]. Gollee and Majschak developed a computer model in order to include the dynamic behavior of the mechanical system in the motion design. For the identification of unknown model parameters, a method based on the process value curve of the motion control system and the measured frame vibration response is proposed [5]. Suárez et al. proposed an experimental mobile manipulator, which is assembled on an omnidirectional platform by a torso with two arms and a human-like structure [6]. Han et al. designed a three-wheeled mobile platform with a three-degree-of-freedom manipulator, constructed its dynamic model, and designed a sliding mode control with kinematics control to follow the design position trajectory of the mobile manipulator. The simulation and experimental results are also compared with the conventional PID algorithm [7]. Min and Liu are based on the inverse method, using only one fuzzy system to approximate the unknown nonlinear function, unknown control gain, and differential of virtual control law of each subsystem. In order to reduce the effect of fuzzy approximation error and external disturbance, the above control scheme is further improved by designing special adjustable control parameters and first-order low-pass filter [8]. The Internet of Things, Earth observation, and large scientific experiments are the sources of today's vast amounts of sensor big data. The standard approach in this case is the stream mining approach, which looks at a particular measurement only once during real-time processing. Based on this, Klemen and Dunja proposed a data cleaning algorithm that can be applied to real-world streaming big data [9, 10]. However, these scholars did not study and discuss the design and operation algorithms of manipulator mechanical systems based on multisensor fusion but only unilaterally analyzed their significance.

3. Method of Manipulator Mechanical System Design and Operation Algorithm

3.1. Big Data Fusion. Data fusion technology is originated in the field of military applications. In the modern warfare system, only sensor information can no longer meet the needs of modern battlefield confrontation. To achieve better combat effects, it is necessary to use various sensor signals and data composed of active and passive detection methods such as infrared, microwave, laser, submillimeter wave, and even electronic intelligence technology. It is precisely with this development trend that big data fusion technology was bred from modern technology and began to develop rapidly. Although the introduction of data fusion technology is easy to understand, the actual data fusion technology is very complicated from scheme design to implementation. Due to the continuous advancement of computer, communication technology, and signal processing technology, many problems in the integration of big data have begun to be gradually overcome. At present, some real-time fusion systems have been put into real-world applications. Figure 1 shows the network structure of the wireless sensor network.

A large number of sensing signals in wireless sensor networks are transmitted from multiple nodes to aggregation nodes. According to the form of signal transmission and the processing level of network nodes, there are usually two types of data fusion modes: distributed and centralized. The distributed structure is also called the intranetwork data fusion structure, as shown in Figure 2. These structures can improve the data acquisition efficiency of the entire network to a certain extent, thereby reducing the amount of data, thereby reducing power consumption, thereby increasing the channel utilization rate, and extending the life of the entire network [11].

The advantage of the centralized architecture is that the source node can directly transmit relevant data to the aggregation node and then realize data fusion by cooperating with the aggregation node. Although this architecture can reduce the signal loss very well, because the nodes of the wireless sensor network are very tightly distributed, many kinds of source nodes will be generated to characterize the data of the same event. In this way, many redundant signals of similar size are produced, and the transmission of redundant signals also needs to consume a lot of power resources of the network [12].

According to the fusion purpose and fusion level, the appropriate fusion algorithm is intelligently selected, and the spatially registered data (or the extracted image features or the attribute description of pattern recognition) are organically synthesized to obtain a more accurate representation or estimation of the target. For the fusion information obtained by various algorithms, sometimes, further processing is required, such as "matching processing" and "type transformation," in order to obtain a more accurate representation or estimation of the target.

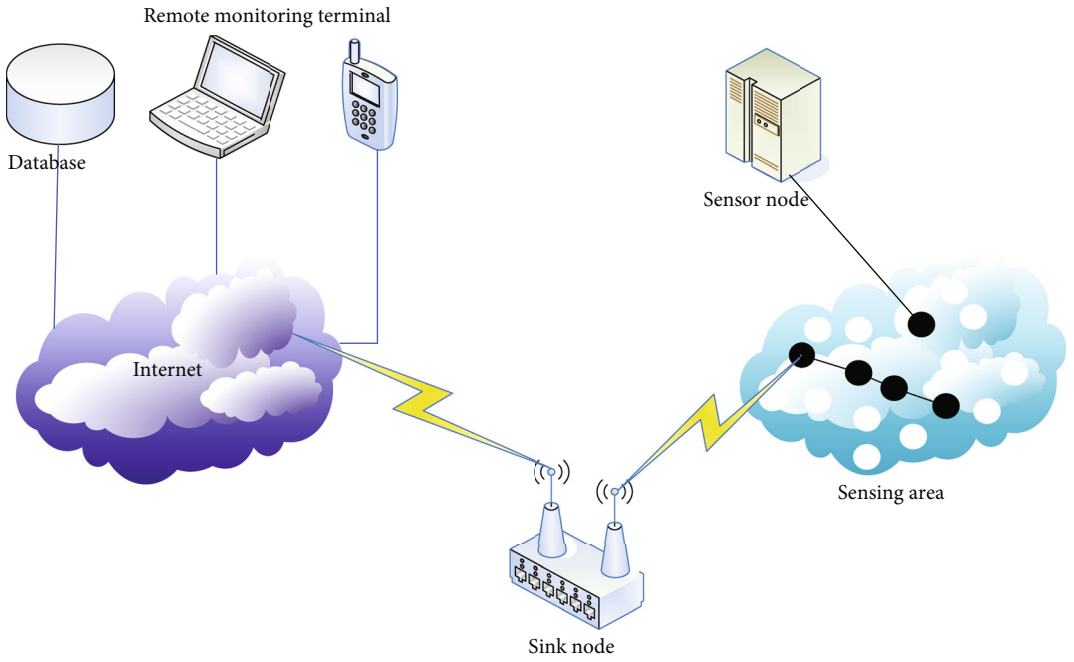

Figure 1: Network structure of wireless sensor network.

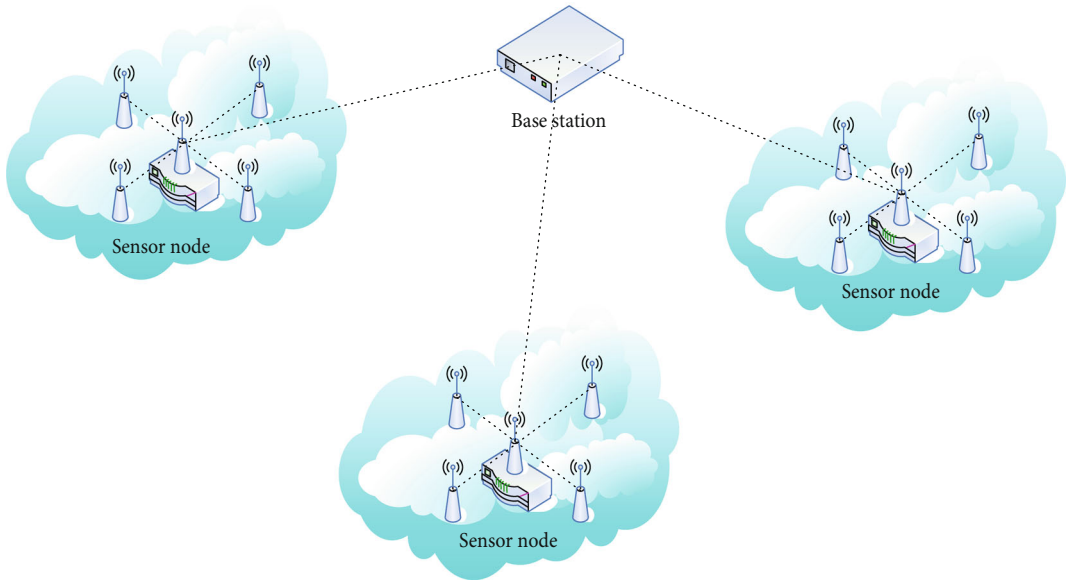

Figure 2: Data fusion model.

3.2. Multisensor Data Fusion Algorithm. The multisensor data fusion algorithm is to realize the mutual fitting of multiple sensor data on the basis of fully considering the characteristics of each sensor in the system. The data fusion algorithm can remove redundant information while retaining complementary information to achieve the best estimation of information [13]. In a multisensor-based detection system, each sensor has a different principle; so, the data calculated from their measured values are not the same. However, the attitude of the carrier at a certain moment is uniquely determined; so, the entire system should eventually output the only accurate measurement value [14]. For the detection results of multiple different sensors, the data fusion algorithm is used to process them to minimize the errors contained in the sensor measurement and calculation process, so as to obtain the optimal estimated value [15]. Currently, the most widely used data fusion algorithms include gradient descent, complementary filtering and Kalman filtering.

3.2.1. Gradient Descent Algorithm. The step descent method is a classic numerical method. In order to obtain the local optimal prediction solution, it can be replaced gradually according to the direction opposite to the gradient of the

objective function, so that the objective function is continuously reduced until it is close to the local minimum. In a comprehensive detection system based on multiple sensors, an objective function is defined for the signals obtained after the solution of each sensor, and continuous iterative operations are performed to obtain the optimal value. Like other data fusion algorithms, its ideas and implementation methods are relatively simple [16, 17].

For the multivariate objective function $g(A)$, assuming that it is defined and differentiable at the point m, it grows most rapidly towards the gradient $\nabla g(m)$ at the point m. On the contrary, along the negative gradient direction $-\nabla g(m)$, $g(A)$ drops the fastest. At this time, if a sufficiently small positive real number$\varphi(\varphi>0)$ is given, it must satisfy

$$g(m) \geq g(m - \varphi * \nabla g(m)). \tag{1}$$

Following this conclusion, in solving for the partial minimum of the target function $g(A)$, it is assumed that starting from the initial estimate a_0 and considering the following $a_0, a_1, \cdots, a_s$ and a_s satisfied

$$a_{s+1} = a_s - \varphi * \nabla g(a_s), a \geq 0. \tag{2}$$

Then, it can get

$$g(a_0) \geq g(a_1) \geq g(a_2) \geq \cdots \tag{3}$$

It is foreseeable that the objective function $g(A)$ will eventually converge and reach the minimum value at a certain point a_h. Figure 3 shows the search path of the gradient descent method.

When using the gradient descent method to fuse data from a three-axis MEMS accelerometer, a three-axis MEMS gyroscope, and a three-axis magnetoresistive sensor, the objective function can be obtained by comparing the angle obtained by the gyroscope with the value obtained by the accelerometer and the magnetoresistive sensor. Using the gravitational field $[0, 0, f]^R$ and the geomagnetic field $[0, t_b, t_j]^R$ at the position of the carrier, the objective function is defined as

$$g(D) = \begin{bmatrix} E_v * \begin{bmatrix} 0 \\ 0 \\ f \end{bmatrix} - \begin{bmatrix} m_a \\ m_b \\ m_j \end{bmatrix} \\ E_v * \begin{bmatrix} 0 \\ t_b \\ t_j \end{bmatrix} - \begin{bmatrix} u_a \\ u_b \\ u_j \end{bmatrix} \end{bmatrix}. \tag{4}$$

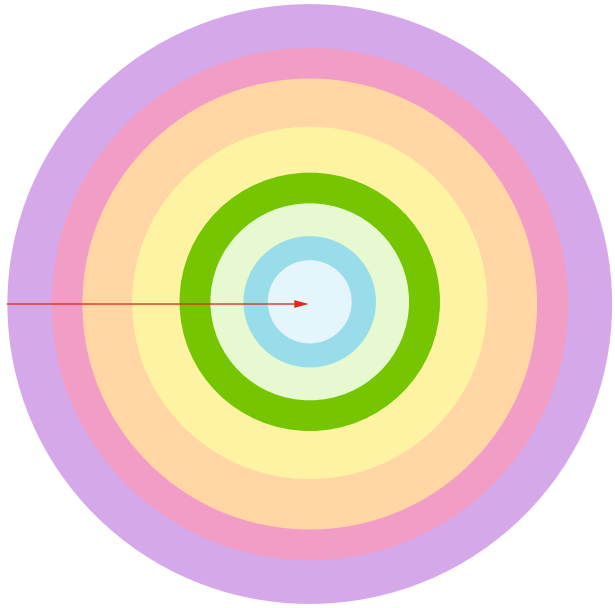

Figure 3: Gradient descent method search path.

The quaternion can be updated as follows:

$$D_h = D_{h-1} + \frac{1}{2} * \begin{bmatrix} 0 & -v_a & -v_b - v_j & \\ v_a & 0 & v_j & -v_b \\ v_b & -v_j & 0 & v_a \\ v_j & v_b & -v_a & 0 \end{bmatrix} * D_{h-1} * \Delta w - \tau \nabla g(D) * \Delta w. \tag{5}$$

In the above formula, Δw is the time interval between two iterative calculations. If the stride length is too short, the conversion rate will be slower, which will affect the real-time performance of the pose calculation [18]. If the stride length is too long, the conversion will oscillate, resulting in the inability to obtain optimal estimates [19].

3.2.2. Complementary Filtering Algorithm. The complementary filtering algorithm is an algorithm in which multiple sets of data are combined and complemented, and the output is stabilized by filtering to obtain the attitude. The complementary filtering algorithm is mainly used to identify distinct noise disturbances from a spectrum domain perspective based on the difference in noise frequencies contained in the detection process of various sensors. The design idea is relatively simple, that is, according to the different frequency domain characteristics of different sensor data, the corresponding filter is used to separate the effective measurement signal and the noise signal of the sensor. Therefore, the algorithm realizes the optimal estimation of information in the frequency domain [20].

These two filters are complementary in terms of frequency. That is, the transfer functions of the two filters satisfy

$$F_1(t) + F_2(t) = 1. \tag{6}$$

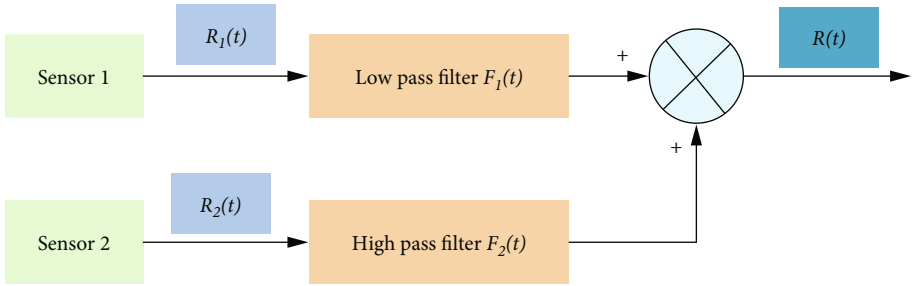

Figure 4: Principle structure diagram of complementary filter.

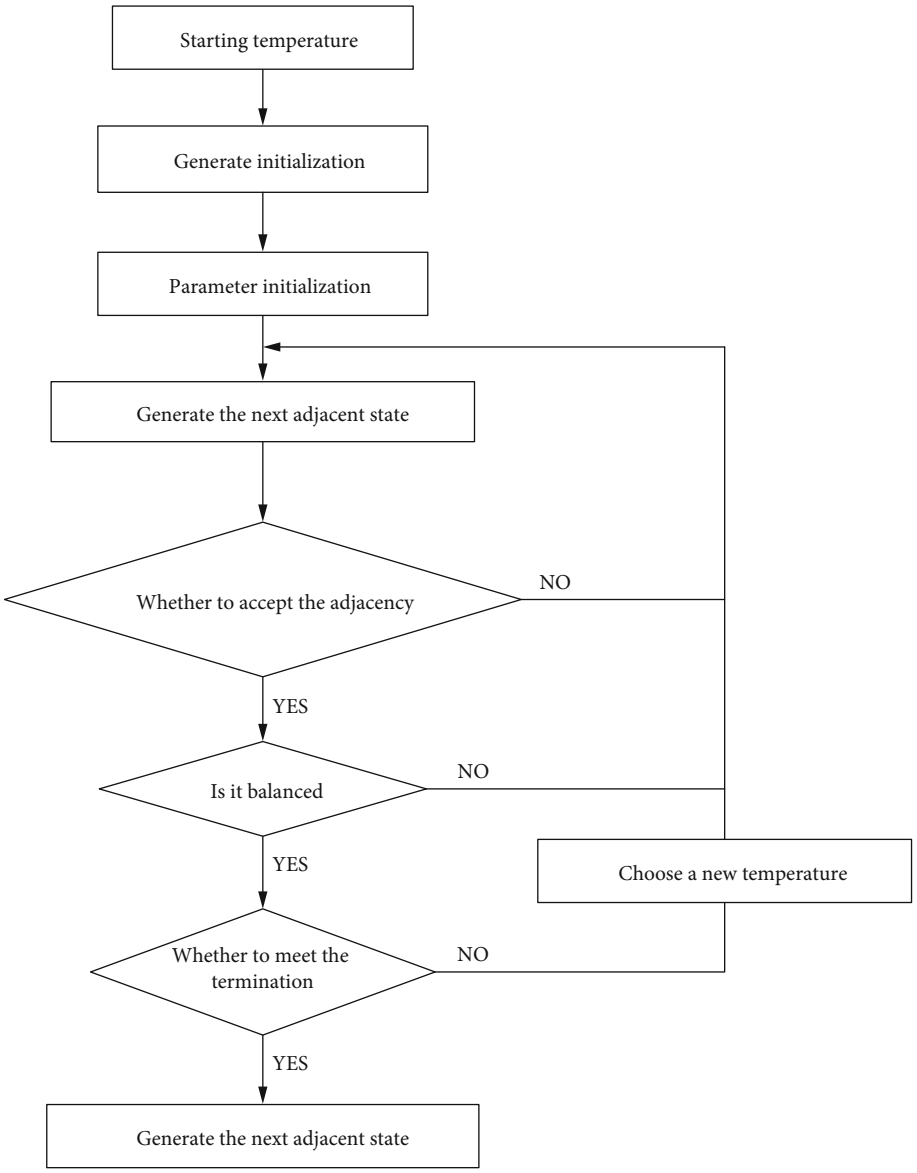

Figure 5: Block diagram of the simulation algorithm.

Table 1: Comparison of data fusion algorithms.

Data fusion algorithm	Fusion accuracy	Amount of calculation	Convergence speed	Requirements for the processor
Gradient descent algorithm	Larger	Small	Slower	Small
Complementary filtering algorithm	Small	Small	Slower	Small
Kalman filter algorithm	Large	Large	Quick	Large

Table 2: Operating parameters of each axis servo motor.

Name	Scope	Mechanical speed	Motor speed	The fastest time of the whole journey
1 axis	-160° ~ +160°	170°/s	1800 rpm	1.5 s
2 axis	0 ~ 1000 mm	400 mm/s	2800 rpm	2.1 s
3 axis	0 ~ 500 mm	400 mm/s	2800 rpm	1.1 s
4 axis	-160° ~ +160°	350°/s	2800 rpm	0.9 s

In the above formula, $F_1(t)$ and $F_2(t)$ are the transfer functions of the low-pass filter and the high-pass filter, respectively. When studying the first-order complementary filter, it can be assumed that $F_1(t)$ and $F_2(t)$ are

$$\begin{aligned} F_1(t) &= \frac{H}{H+t}, \\ F_2(t) &= \frac{t}{H+t}. \end{aligned} \tag{7}$$

By examining the rest and motion behavior of various sensors, it is possible to get various sensor data with different frequency domain characteristics, transforming the measured sensor signal from the time domain to the frequency domain for analysis to obtain its specific noise characteristics. Based on if the sensor signature includes HF or LF noise, a certain filter is selected in the supplementary filter to eliminate the appropriate noise, and eventually, the multiple filtered signals are summed to obtain the valid signal of the whole spectrum band, completing the whole denoising and fusion process.

Assuming that the detection system contains two sensors, and their exit values include LF noise and HF noise, respectively, the information obtained by their solution in the frequency domain is $R_1(t)$ and $R_2(t)$, respectively. If the true information is $R(t)$, the following relationship exists:

$$\begin{aligned} R_1(t) &= R(t) + w_K(t), \\ R_2(t) &= R(t) + w_D(t). \end{aligned} \tag{8}$$

In the formula, $w_K(t)$ and $w_D(t)$ are the effects of LF and HF noise signals in the output value on the attitude. At this time, through a complementary filter in Figure 4, the estimated value can be obtained:

$$\begin{aligned} \widehat{R}(t) &= (R(t) + w_K(t))\frac{t}{t+H} + (R(t) + w_D(t))\frac{H}{H+s} \\ &= R(t) + w_K(t) \bullet \frac{t}{t+H} + w_D(t) \bullet \frac{H}{H+s} \approx R(t). \end{aligned} \tag{9}$$

In the formula, $\widehat{R}(t)$ is the estimated value after the complementary filter processing. It can be seen that the supplemental filtering technique can quickly remove the HF or LF noise contained in different sensor signals and finally achieve the purpose of fusing different characteristic data.

Data from the gas pedal and reluctance sensors have been reliable; however, they are vulnerable to the negative effects of outside interference. And because the gyroscope data analysis is highly dynamic, the accuracy is also high in the short term, but its accuracy error will increase with the continuous increase in duration, thus forming a drift phenomenon. Thus, by using the export properties of the three sensors, the HF noise included in the analysis of the acceleration meter and reluctance sensor data is eliminated by using complementary filters. At the same time, the LF noise included in the data analysis of the gyroscope is eliminated, the useful signals in the data analysis of the three are saved, and finally, the accuracy value is obtained through the calculation. After converting to the time domain using the backward difference method, we can get

$$\begin{aligned} \widehat{\alpha}_s &= H_1 * \alpha_{\text{acc}} + (1 - H_1) * (\widehat{\alpha}_{s-1} + v_b * \text{ds}), \\ \widehat{\beta}_s &= H_2 * \beta_{\text{acc}} + (1 - H_2) * (\widehat{\alpha}_{s-1} + v_a * \text{ds}), \\ \widehat{\gamma}_s &= H_3 * \gamma_{\text{mag}} + (1 - H_3) * \left(\widehat{\alpha}_{s-1} + v_j * \text{ds}\right). \end{aligned} \tag{10}$$

From the above formula, we can get that the supplementary filtering method is to trust the gyroscope data for a brief period of time and add the acceleration and reluctance sensor data to modify the gyroscope data to get the correct information.

3.2.3. Kalman Filter Algorithm. Kalman filtering is a method for calculating autonomous regression data with optimized, which can give the best solution in most usage scenarios. Its biggest advantage is that it can truly predict the state of the current system and use a recursive algorithm to correct the a priori estimate of the current state through new observables, thereby improving the characteristics of the filter. Its limitation is that the target tracking is lost when the moving target is occluded for a long time.

The basic idea of the Kalman filter calculation is to take the form of a time-recursive operation. And the estimated

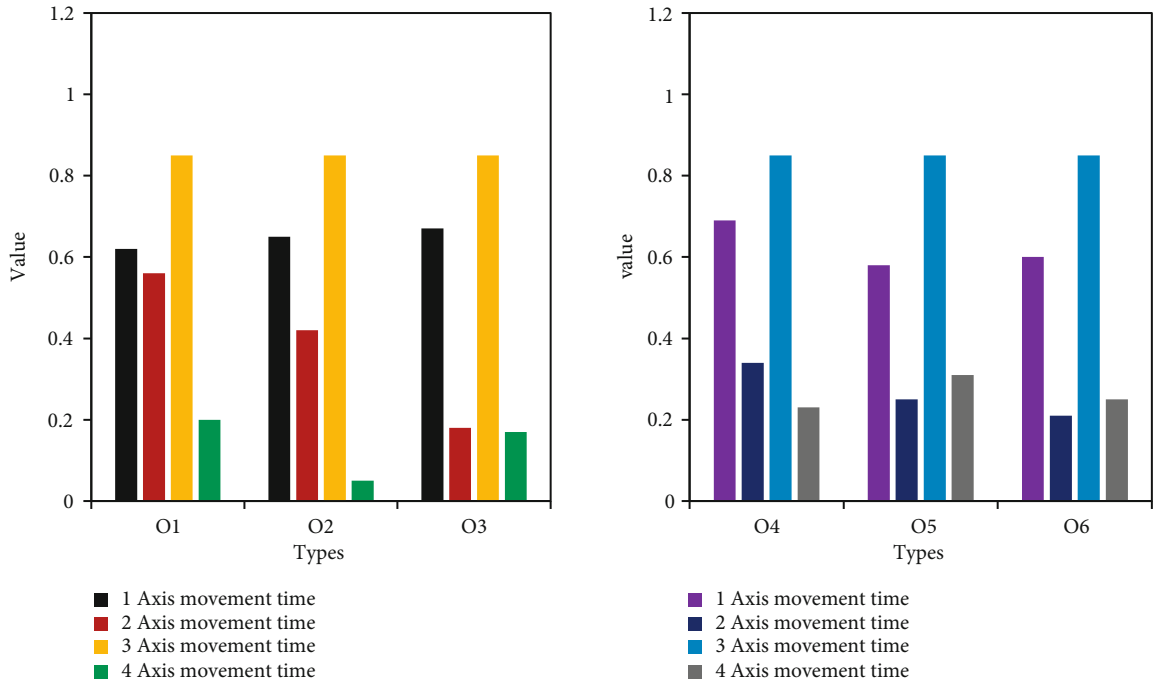

Figure 6: Motion time of each axis of the manipulator 1.

value of the current time is obtained by the optimal estimation principle of minimizing the mean square error. The calculation process must establish two formulas for system design and measurement, as shown below:

$$\begin{aligned} a_h &= M_h * a_{h-1} + D_h * r_h + v_h, \\ j_h &= L_k * a_h + t_h. \end{aligned} \tag{11}$$

In the formula, a_h is the state vector of the system at time h, M_h is the system state transition matrix, D_h is the input conversion matrix of the system, r_h is the control quantity of the system at time h, v_h is the system noise, j_h is the observed measurement of the system at time h, L_k is the conversion matrix measured by the system, and t_h is the observed noise. Assuming that v_h and t_h are mutually independent and normally distributed white noises, we can get

$$\begin{aligned} v_h &\sim N(0, G_h), \\ t_h &\sim N(0, S_h). \end{aligned} \tag{12}$$

The Kalman filter calculation method is to use the system differential formula to perform a priori estimation of the state vector under the premise of the establishment of the above formula. Then, use the measurement differential formula to correct the prior estimation and then perform the posttest estimation of the state vector. Therefore, the Kalman filter algorithm includes two parts: the time update formula and the measurement time update formula in each cycle. The time update formula also includes the following:

$$\hat{a}_{h|h-1} = M_h * \hat{a}_{h-1|h-1} + D_h * r_k, \tag{13}$$

$$C_{h|h-1} = M_h * C_{h-1|h-1} * M_h^S + G_h. \tag{14}$$

Formula (13) is mainly to obtain the priori estimate $\hat{a}_{h|h-1}$ of the current state, and formula (14) calculates its prior covariance $C_{h|h-1}$, both of which are preparations for the measurement update equation. The measurement update formula is as follows:

$$H_h = C_{h|h-1} * L_h^S * \left(L_h * C_{h|h-1} * L_h^S + R_h\right)^{-1}, \tag{15}$$

$$\hat{a}_{h|h} = \hat{a}_{h|h-1} + H_h * \left(j_h - L_h * \hat{a}_{h|h-1}\right), \tag{16}$$

$$C_{h|h} = (I - H_h * L_h) * C_{h|h-1}. \tag{17}$$

Formula (15) calculates the Kalman gain H_h according to the prior covariance $C_{h|h-1}$, and formula (16) uses the Kalman gain H_h and the measured value j_h to compensate the prior state estimate $\hat{a}_{h|h-1}$, so as to obtain the posterior state estimate $\hat{a}_{h|h}$.

When the system uses the Kalman filter algorithm to integrate three-axis MEMS accelerometer, three-axis MEMS gyroscope, and three-axis magnetoresistive sensor data, the system rotation speed signal obtained by the three-axis MEMS gyroscope can be used to form the system state formula as shown below:

$$\begin{bmatrix} \alpha_h \\ \Delta v_h \end{bmatrix} = \begin{bmatrix} 1 & -ds \\ 0 & 1 \end{bmatrix} \begin{bmatrix} \alpha_{h-1} \\ \Delta v_{h-1} \end{bmatrix} + \begin{bmatrix} v_h * ds \\ 0 \end{bmatrix} + \begin{bmatrix} v_\alpha \\ v_v \end{bmatrix}. \tag{18}$$

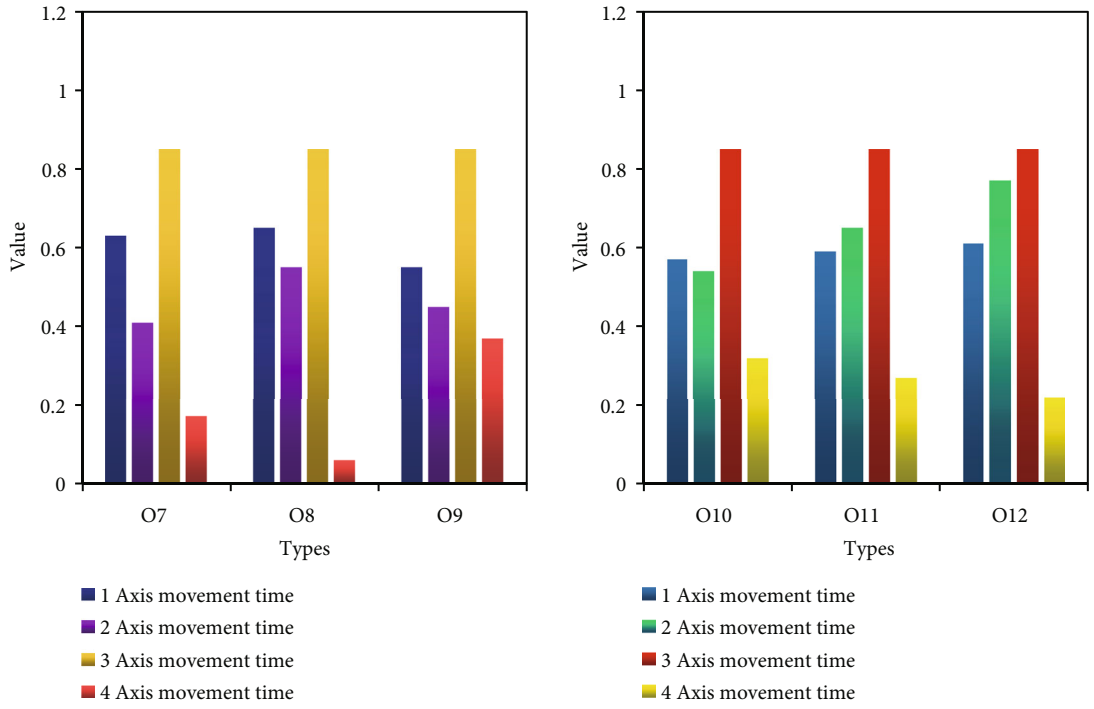

Figure 7: Motion time of each axis of the manipulator 2.

In the formula, α_{h-1} is the optimal estimate at $h-1$, and Δv_{h-1} is the optimal estimate of the gyroscope output error at $h-1$. α_h and Δv_h are the priori estimates of the attitude angle and gyroscope error at time h, respectively. v_h is the output value of the gyroscope, and v_α and v_v are the system noise.

3.2.4. Simulated Annealing Algorithm. In the past, the way we used the local search algorithm to deal with the problem is the following: starting from the initial point, choose the descending direction to search, it seems that this can quickly solve the problem. However, although the local search algorithm is a practical approximation algorithm, this method can only solve the local minimum but cannot obtain the global optimal solution.

The study of solid annealing process gives people new inspiration. First, the similarities exist between the solid annealing process and the combinatorial optimization problem. Simulation of the process of reaching thermal equilibrium in the presence of a solid at a constant temperature is as follows: introducing the Metropolis criterion into the optimization process. Finally, an iterative combinatorial optimization method for the criterion Metropolis algorithm is obtained. This algorithm simulates the solid annealing process, which is called simulated annealing algorithm.

The general algorithm of simulated annealing is shown in Figure 5.

3.3. Comparison of Data Fusion Algorithms. The three algorithms of gradient descent, complementary filtering algorithm, and Kalman filtering algorithm can all realize the fusion processing of acceleration, angular velocity, and magnetic field strength data and obtain unique angular information, but the design ideas of the three are different, and the applicable systems are also different. It is necessary to select a suitable data fusion algorithm according to the actual situation to achieve the optimal estimation of the posture. In the multisensor-based detection system, three typical data fusion algorithms are compared, and the results are shown in Table 1.

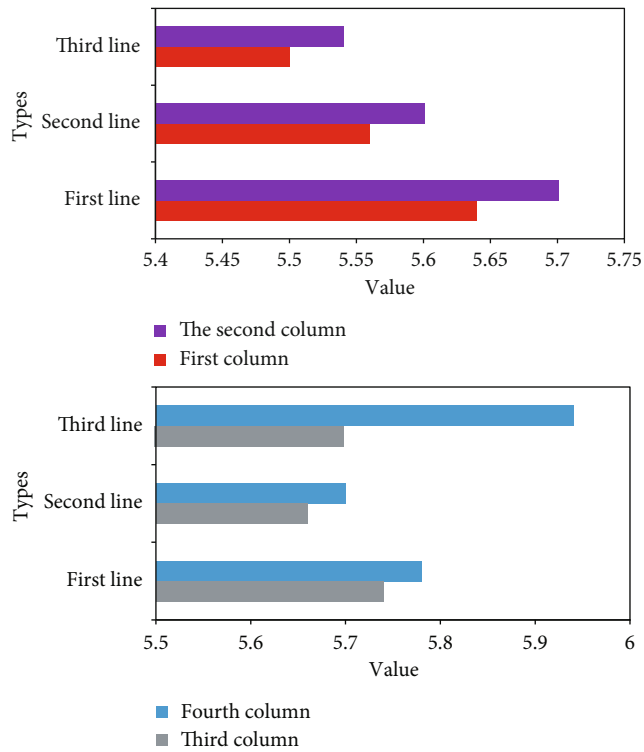

Figure 8: The time it takes to place each box on the first layer.

Table 3: Operating parameters of each axis of the manipulator at 50% rated speed.

Name	Rotating speed	Mechanical speed	Acceleration time	Acceleration	Accelerated displacement
1 axis	900 rpm	90°/s	0.15 s	450°/s^2	8°
2 axis	1300 rpm	240 mm/s	0.2 s	900 mm/s^2	30 mm
3 axis	1300 rpm	240 mm/s	0.2 s	900 mm/s^2	30 mm
4 axis	1300 rpm	80°/s	0.25 s	250°/s^2	12°

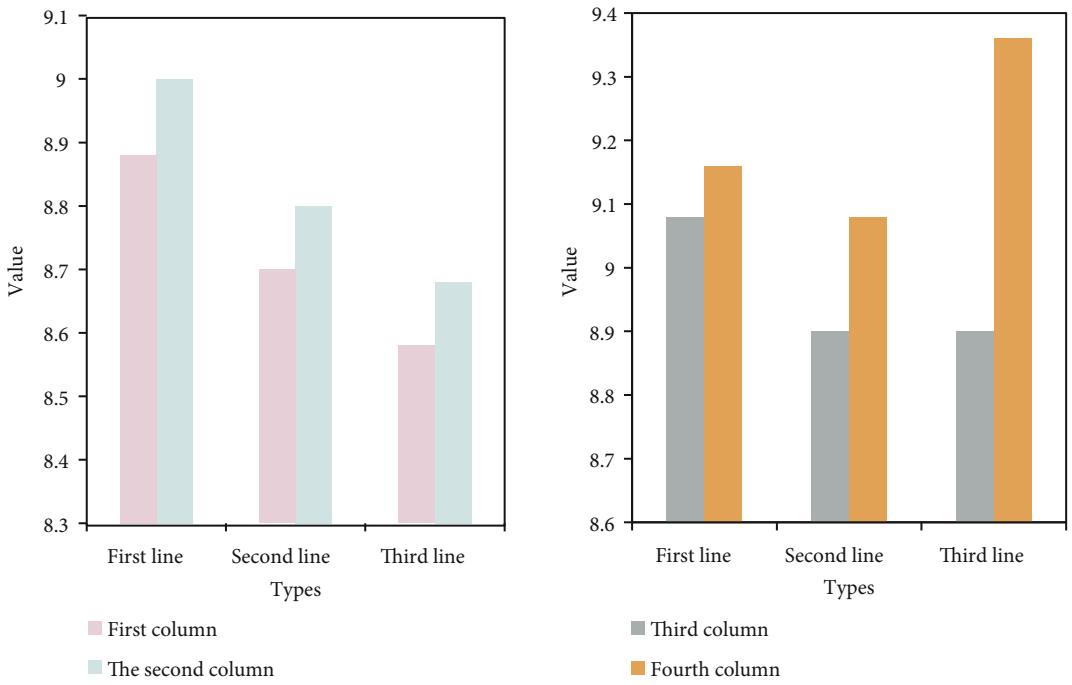

Figure 9: Required time.

It can be obtained from Table 1 that among the three algorithms, the complementary filtering algorithm has lower fusion accuracy and slower convergence speed than the other two algorithms. Therefore, the overall performance is not good, but its calculation amount is small, and the requirements for the processor are low. Therefore, this algorithm can be selected to process sensor data in an attitude detection system with limited hardware performance and low accuracy requirements. Compared with the gradient descent method, the Kalman filter algorithm obtains more accurate information value and has a good convergence speed. But at the same time, the Kalman filter algorithm contains complex matrix operations; so, a lot of calculations are required, and the performance requirements of the processor are relatively high. In the case of hardware support, the Kalman filter algorithm could select to enhance the whole system detection performance.

4. Experimental Results

4.1. The Rated Motion Parameters of Each Axis Motor of the Manipulator. When the manipulator is running, the program sets 1, 2, and 4 axes to rotate at the same time, moving directly above the center of the packaging box or carton. After the 1, 2, and 4 axes are in place, the 3 axis drives the gripper to move vertically downward. When the diffusion photoelectric switch on the gripper is triggered, the 3 axis stops moving.

The operating parameters of each axis servo motor of the manipulator in this design are shown in Table 2. Table 2 has the rated speed of each axis servo motor, the mechanical speed of each axis, the range of motion, and the fastest motion time of the whole process.

The movement time of each axis of the manipulator is shown in Figures 6 and 7 In order to prevent the manipulator from touching obstacles in the assembly line or packing box station during the packing process, each time the box is packed, the 3-axis first moves down to the packing box station or the carton placement coordinate point and grabs or places the packing box. After grabbing or placing, the 3 axis moves up again.

When the manipulator is packing and running, the program sets axis 1, 2, and 4 to rotate at the same time, and axes 1, 2, and 4 move directly above the packing box placement station at the same time. After axis 1, axis 2, and axis 4 are all in place, axis 3 drives the gripper to move vertically downward. When the diffusion photoelectric switch on the gripper is triggered, the 3-axis stops moving, and the gripping electromagnet starts to clamp the packaging box. After

Table 4: Operating parameters of 60% rated speed of each axis of the manipulator.

Name	Rotating speed	Mechanical speed	Acceleration time
1 axis	1000 rpm	100°/s	0.15 s
2 axis	1600 rpm	270 mm/s	0.2 s
3 axis	1600 rpm	270 mm/s	0.2 s
4 axis	1600 rpm	96°/s	0.25 s

clamping, the 3-axis drives the gripper to lift up 300 mm vertically. After the movement is in place, the 3-axis stops moving. Then, axis 1, axis 2, and axis 4 move directly above the packing box placement station at the same time. After axis 1, axis 2, and axis 4 are all in place, stop at the place where the box is placed, complete one boxing action, and wait for the next boxing work. The time taken to place each packaging box on the first layer is shown in Figure 8.

It can be seen from Figure 8 that the average time required for the manipulator to place a packaging box is 5.67 s. It is less than the requirement that the time given by the company to place a packaging box is less than 8 s, and it meets the technical indicators required by the company, indicating that the mechanical arm of this design meets the requirements.

4.2. Movement of Each Axis Motor of the Manipulator at Nonrated Speed. When the motor speed of each axis of the manipulator is set to 50% of the rated speed, the rated speed of the servo motor of the manipulator 1 axis is 900 rpm, and the mechanical speed of the 1 axis is 90°/s. In this design, the operating parameters of each axis of the manipulator at 50% of the rated speed are shown in Table 3.

Assuming that the clamping and unclamping time tc of the gripping electromagnet are both 0.5 s, the time used to place each packaging box of the first layer is shown in Figure 9.

It can be seen from Figure 9 that the average time required for the manipulator to place a packaging box is 8.93 s. It is less than the requirement that the time given by the company to place a packaging box is less than 8 s, and it meets the technical indicators required by the company, indicating that the mechanical arm of this design meets the requirements.

When the rotation speed of each axis motor of the robot is set to 60% of the rated rotation speed, the rated rotation speed of the servo motor of the robot 1 axis is 1000 rpm. The operating parameters of the 60% rated speed of each axis of the manipulator in this design are shown in Table 4.

Assuming that the clamping and unclamping time tc of the gripping electromagnet are both 0.5 s, the movement time of each axis at 60% of the rated speed of each axis of the manipulator is calculated according to the above calculation method. The time taken to place each packaging box on the first layer is shown in Figure 10.

It can be seen from Figure 10 that the average time required for the manipulator to place a packaging box is 7.84 s. It is less than the requirement that the time given by

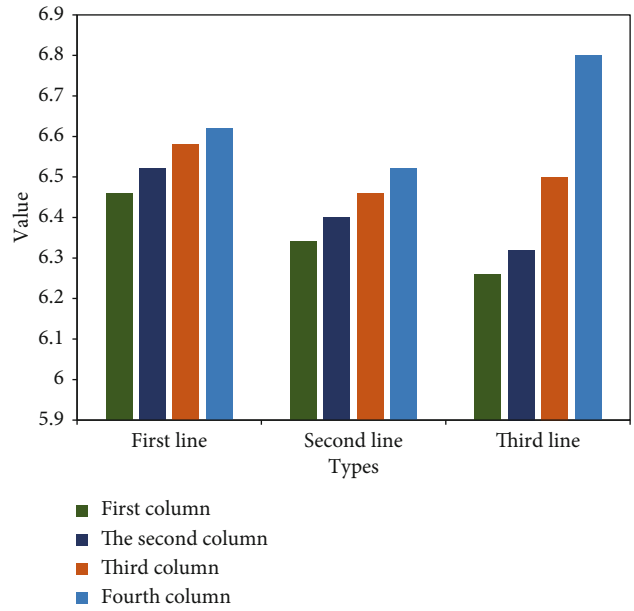

Figure 10: Elapsed time.

the company to place a packaging box is less than 8 s, and it meets the technical indicators required by the company, indicating that the mechanical arm of this design meets the requirements.

5. Discussion

The robot hand is usually composed of three parts: the hand, the movement organization, and the controller. Robotic hand refers to the mechanical part used to grasp the work (or utensil), and it has many forms according to the shape, width, specific gravity, material, and operation needs of the grasped object. In the movement mechanism, the robot hand can perform various methods such as rotation (swing), movement, or compound body movement to obtain the actions regulated by the mechanism and thereby adjust the body parts and posture of the grasped object. The independent motion methods such as ups and downs, extensions, and rotations of the motion mechanism are called the degrees of freedom of motion of the robot hand. The degree of freedom is also an important reference for the design of the robot hand. The more freedom of movement, the greater the sensitivity of the manipulator, the wider the versatility, the more complex structure, the more cumbersome processing, and the correspondingly higher economic value. Usually, a dedicated robot has 2 to 3 degrees of freedom. The controller generally uses the control of the generator on each synovial joint of the robot to carry out a certain order of dynamics. At the same time, it receives the information reflected by the photoelectric encoder to form a stable closed-loop control system. The core of the controller is usually made up of microcontrollers such as single-chip microcomputers and dsp, and the required control performance is achieved through its programming.

6. Conclusion

The development of science and technology also promotes the progress of society, making automatic control more used in people's daily life and working environment. When people are no longer competent in certain areas of work, robots also follow. Manipulators are not only the first industrial robots produced by mankind but also the first modern robots produced by mankind. It can replace ordinary people's tedious work and highly repetitive working environment to achieve a high degree of mechanization and automation of industrial products and can operate normally under unfavorable working environments to protect workers' lives. The manipulator has developed very fast in recent years. It has greatly improved its palletizing load, operating speed, and adjustment accuracy, but its value has continued to decline. The robot hand has been more and more commonly used in various industries, and it has exerted more and more advantages in the palletizing process. With the large-scale application of manipulators in life and product production, people's living standards and productivity have been greatly improved, and people's working environment has also been changed. With the modernization of product production and lifestyle, the scope of use of manipulators will also have a wider space for development.

Data Availability

The data used to support the findings of this study are available from the corresponding author upon request.

Conflicts of Interest

The authors declare no conflicts of interest.

References

[1] W. Yi, M. Jiang, R. Hoseinnezhad, and B. Wang, "Distributed multi-sensor fusion using generalised multi-Bernoulli densities," *Iet Radar Sonar & Navigation*, vol. 11, no. 3, pp. 434–443, 2017.

[2] K. Lu and R. Zhou, "Multi-sensor fusion for robust target tracking in the simultaneous presence of set-membership and stochastic Gaussian uncertainties," *Iet Radar Sonar & Navigation*, vol. 11, no. 4, pp. 621–628, 2017.

[3] E. Benli, R. L. Spidalieri, and Y. Motai, "Thermal multisensor fusion for collaborative robotics," *IEEE Transactions on Industrial Informatics*, vol. 15, no. 7, pp. 3784–3795, 2019.

[4] S. Shi, H. Wu, Y. Song, and H. Handroos, "Mechanical design and error prediction of a flexible manipulator system applied in nuclear fusion environment," *Industrial Robot: An International Journal*, vol. 44, no. 6, pp. 711–719, 2017.

[5] C. Gollee and J. P. Majschak, "A parameter identification case-study for a dynamical mechanical system using frequency response analysis and a particle swarm algorithm for trajectory optimization," *Engineering Science and Technology, an International Journal*, vol. 23, no. 4, pp. 769–780, 2020.

[6] R. Suárez, L. Palomo-Avellaneda, J. Martinez, D. Clos, and N. García, "Development of a dexterous dual-arm omnidirectional mobile manipulator," *IFAC-Papers OnLine*, vol. 51, no. 22, pp. 126–131, 2018.

[7] S. Han, H. Ha, Y. Zhao, and J. Lee, "Assumed model feedforward sliding mode control for a wheeled mobile robot with 3-DOF manipulator systems," *Journal of Mechanical Science & Technology*, vol. 31, no. 3, pp. 1463–1475, 2017.

[8] W. Min and Q. Liu, "An improved adaptive fuzzy backstepping control for nonlinear mechanical systems with mismatched uncertainties," *Automatika*, vol. 60, no. 1, pp. 1–10, 2019.

[9] K. Klemen and M. Dunja, "Autonomous sensor data cleaning in stream mining setting," *Business Systems Research Journal*, vol. 9, no. 2, pp. 69–79, 2018.

[10] I. Svalina, S. Havrlišan, K. Šimunović, and T. Šarić, "Investigation of correlation between image features of machined surface and surface roughness," *Tehnicki vjesnik-Technical Gazette*, vol. 27, no. 1, pp. 27–36, 2020.

[11] M. Rick, J. Clemens, L. Sommer, A. Folkers, K. Schill, and C. Büskens, "Autonomous driving based on nonlinear model predictive control and multi- sensor fusion," *IFAC-PapersOnLine*, vol. 52, no. 8, pp. 182–187, 2019.

[12] J. Yan, Z. Xu, X. Luo, C. Chen, and X. Guan, "Feedback-based target localization in underwater sensor networks: a multisensor fusion approach," *IEEE Transactions on Signal and Information Processing over Networks*, vol. 5, no. 1, pp. 168–180, 2019.

[13] I. Aydin, S. B. Celebi, S. Barmada, and M. Tucci, "fuzzy integral-based multi-sensor fusion for arc detection in the pantograph-catenary system," *Journal of rail and rapid transit*, vol. 232, no. 1, pp. 159–170, 2018.

[14] R. R. Alvarado and E. C. Castaeda, "Optimum design of the reconfiguration system for a 6-degree-of-freedom parallel manipulator via motion/force transmission analysis," *Journal of Mechanical Science and Technology*, vol. 34, no. 3, pp. 1339–1349, 2020.

[15] S. A. Krasnova and A. S. Antipov, "Hierarchical design of Sigmoidal generalized moments of manipulator under uncertainty," *Automation & Remote Control*, vol. 79, no. 3, pp. 554–570, 2018.

[16] S. Yu, J. Lee, B. Park, and K. Kim, "Design of a gripper system for tendon-driven telemanipulators considering semi-automatic spring mechanism and eye-in-hand camera system," *Journal of Mechanical Science and Technology*, vol. 31, no. 3, pp. 1437–1446, 2017.

[17] Y. Zhang, X. Luo, C. Zhu, W. Lu, and X. Wang, "Optimization of gait parameters for energy efficiency improvement of farmland robot based on orthogonal experiment design," *Tehnicki vjesnik-Technical Gazette*, vol. 26, no. 3, pp. 703–709, 2019.

[18] W. Alam, A. Mehmood, K. Ali, U. Javaid, S. Alharbi, and J. Iqbal, "Nonlinear control of a flexible joint robotic manipulator with experimental validation," *Journal of Mechanical Engineering*, vol. 64, no. 1, pp. 47–55, 2018.

[19] B. Altiner, A. Delibasi, and B. Erol, "Modeling and control of flexible link manipulators for unmodeled dynamics effect," *Proceedings of the Institution of Mechanical Engineers*, vol. 233, no. 3, pp. 245–263, 2019.

[20] M. Hadi Barhaghtalab, V. Meigoli, M. R. Golbahar Haghighi, S. A. Nayeri, and A. Ebrahimi, "Dynamic analysis, simulation, and control of a 6-DOF IRB-120 robot manipulator using sliding mode control and boundary layer method," *Journal of Central South University*, vol. 25, no. 9, pp. 2219–2244, 2018.